Sustainable Energy & Fuels

Low-Spin Cobalt(II) Redox Shuttle by Isocyanide Coordination

Journal:	*Sustainable Energy & Fuels*
Manuscript ID	SE-ART-02-2020-000314
Article Type:	Paper
Date Submitted by the Author:	26-Feb-2020
Complete List of Authors:	Raithel, Austin; Michigan State University, Chemistry Kim, Tea-Yon; Michigan State University, Chemistry Nielsen, Karl; Michigan State University, Chemistry Staples, Richard; Michigan State University, Chemistry Hamann, Thomas; Michigan State University, Chemistry

Low-Spin Cobalt(II) Redox Shuttle by Isocyanide Coordination

Austin L. Raithel, Tea-Yon Kim, Karl Nielsen, Richard J. Staples and Thomas W. Hamann

Department of Chemistry, Michigan State University, East Lansing, Michigan 48824, United States

KEYWORDS: Low-spin, cobalt complex, redox shuttle, dye-sensitized solar cells

Abstract

Coordination of the strong-field ligand 2,6-dimethylphenyl isocyanide (DMP-CN) to the Co(PY5Me$_2$) framework, where PY5Me$_2$ represents the pentadentate ligand 2,6-bis(1,1-bis(2-pyridyl)ethyl)pyridine, has resulted in a new low-spin Co(II) complex with a relatively low reorganization energy and fast electron-transfer kinetics compared to the prototypical cobalt tris-bipyridine redox shuttle, $[Co(bpy)_3]^{3+/2+}$, where bpy represents 2,2'-bipyridine. Despite nearly 160 mV reduced regeneration driving force, the $[Co(PY5Me_2)(DMP\text{-}CN)]^{3+/2+}$ redox shuttle displayed an increased regeneration efficiency relative to $[Co(bpy)_3]^{3+/2+}$, however recombination losses hinder the performance as evidenced by a reduced recombination resistance. Future directions point to low-spin Co(II) redox shuttles with more negative redox potentials to be paired with a dye or dye mixture that absorbs into the near infrared region.

Introduction

Dye-sensitized solar cells, DSSCs, remain a promising solar energy conversion technology. Through continued optimization of the photoanode, dye, redox shuttle and counter electrode, DSSCs have recently reached reported power conversion efficiencies greater than 14% under AM 1.5 illumination, 32% under 1000 lux illumination as well as a certified efficiency of 12%.[1,2,3,4] The first major successes came from a small class of ruthenium sensitizers with long excited state lifetimes and broad absorbance across the visible spectrum.[5,6] These systems performed well when paired with the iodide/triiodide electrolyte, but had several inherent drawbacks. Primarily, a large overpotential was required to efficiently regenerate these dyes due to the multi-electron transfer pathway of the redox shuttle.[7,8] In order to reduce the voltage loss of the devices, one electron outer-sphere redox couples have been used to efficiently reduce the oxidized sensitizers. The most successful of these redox couples have been cobalt and copper based redox shuttles that display near unity dye regeneration with less required driving force than iodide.[9,10] By tuning the ligand scaffold of these complexes, the redox potentials have been optimized to produce the maximum photovoltage while still efficiently regenerating the sensitizers.

The reorganization energy is a key parameter that should allow for further optimization of the charge-transfer kinetics in a DSSC. It has been shown previously that cobalt redox couples typically have a large inner-sphere reorganization energy due to the structural changes associated with the high-spin Co(II) to low-spin Co(III) electronic configuration change during electron transfer.[11] In order to reduce the electron transfer barrier, we have investigated use of strong-field ligands to induce a low-spin electronic configuration of Co(II) metal centers.[12] For example, $[Co(ttcn)]^{3+/2+}$ displayed improved dye regeneration kinetics over the high performing redox

couple $[Co(bpy)_3]^{3+/2+}$ despite 50 mV less driving force for regeneration.[13] However, the redox couple suffered from greater recombination losses due to the smaller inner-sphere reorganization energy which resulted in nominally the same power conversion efficiency. While the $[Co(ttcn)]^{3+/2+}$ redox shuttle has some promising attributes, it is limited by not being amenable to manipulation of redox potential through modification of the ligand framework. There are very few other reported examples of low-spin Co(II) complexes which are viable alternative redox shuttles for DSSCs.

In order to develop a new family of low-spin Co(II) complexes, where the redox potential can be tuned, we turned to the $PY5Me_2$ ligand, where $PY5Me_2$ represents the pentadentate ligand 2,6-bis(1,1-bis(2-pyridyl)ethyl)pyridine.[14] Some $[Co(PY5Me_2)(L)]^{3+/2+}$ redox couples have been used previously in dye-sensitized solar cells, but these works involved relatively small perturbations in the redox potential by coordination of bases commonly used in the electrolyte, and no examples of low-spin Co(II) complexes.[15] Our group attempted to develop a new low-spin Co(II) redox shuttle by cyanide coordination to the $PY5Me_2$ framework.[16] Unfortunately, the cyanide ligand acted as a bridging unit to form dimer and cluster complexes in solution which prohibited the redox shuttle from being used in full devices. In this work, the strong-field ligand 2,6-dimethyphenyl isocyanide (DMP-CN) was coordinated to the $[Co(PY5Me_2)(L)]^{3+/2+}$ couple to result in a new low-spin Co(II) redox shuttle. This allowed for further study between the balance of redox potential and reorganization energy and their effects on the kinetics of electron transfer in DSSCs.

Experimental

Materials

All chemicals were either purchased from commercial suppliers or synthesized from commercially available reagents. 2-ethyl pyridine, 2-fluoropyridine and 2,6-difluoropyridine were purchased from oakwood chemical and used as received. Acetonitrile-d3, EDOT, and sodium dodecyl sulfate were purchased from MilliporeSigma. Tert-butyl alcohol was purchased from Alfa Aesar and used as received. $PY5Me_2$ (2,6-bis(1,1-bis(2-pyridyl)-ethyl)pyridine) was synthesized as reported previously.[14] Tris(4-bromo-phenyl)amine was purchased from TCI America and used as received. Tris(4-bromo-phenyl)amine hexafluorophosphate [TBPA](PF_6) was synthesized by modifying a previous preparation as described below.[17] Dimethyl phenyl isocyanide was synthesized as described previously, and purified by recrystallizing twice from hot hexanes by cooling in a freezer.[18] Thallium hexafluorophosphate was obtained from STREM chemical and used as received. Nitrosonium hexafluorophosphate was purchased from Fisher Scientific and used as received. The D35cpdt dye, 3-{6-{4-[bis(2',4'-dibutyloxybiphenyl-4-yl)amino-]phenyl}-4,4-dihexyl-cyclopenta-[2,1-b:3,4-b']dithiophene-2-yl}-2-cyanoacrylic acid, was purchased from Dyenamo and used as received. Chenodeoxycholic acid and 25 μm surlyn were purchased from Solaronix and used as received. $[Co(bpy)_3](PF_6)_2$ and $[Co(bpy)_3](PF_6)_3$ were synthesized using previously established procedures.[12] $[Co(PY5Me_2)(I)]I$ and $[Co(PY5Me_2)(ACN)](PF_6)_2$ were synthesized as listed previously except the reaction time was shortened to 16 hours for both complexes.[19] All $[Co(PY5Me_2)(L)]$ complexes were synthesized in a nitrogen filled glovebox.

Synthesis

$[Co(PY5Me_2)(ACN)](PF_6)_3$ Synthesis

$[Co(PY5Me_2)(ACN)](PF_6)_2$ (0.12 mmol, 0.100 g) was weighed into a 20 mL vial. [TBPA](PF_6) (0.12 mmol, 0.075 g) was weighed into a separate 20 mL vial then quantitatively transferred with 3 × 1 mL portions of dry acetonitrile. The solution immediately turned dark red with a white

precipitate. After stirring for 2 hours, 18 mL of dry dichloromethane was added to dissolve the white solid and precipitate a red-brown solid product. The solvent was decanted and the solid was washed with 3 × 1 mL portions of dry DCM (yield: 0.107 g, 91.3%). ^{1}H NMR (500 MHz, acetonitrile-d3) δ 9.53 (d, J = 6.3 Hz, 4H), 8.38 – 8.31 (m, 1H), 8.29 – 8.22 (m, 8H), 8.17 (dd, J = 8.1, 1.5 Hz, 4H), 7.89 – 7.82 (m, 4H) 2.87 (s, 6H). Elemental analysis: found (calculated) for $Co(PY5Me_2)(ACN)(PF_6)_3$, $C_{31}H_{28}CoF_{18}N_6P_3$: C, 37.89(38.05); H, 3.04(2.88); N, 7.79(8.59).

[Co(PY5Me$_2$)(DMP-CN)](PF$_6$)$_2$ Synthesis

$[Co(PY5Me_2)(ACN)](PF_6)_2$ (0.88 mmol, 0.734 g) was weighed into a 20 mL vial. Dimethyl phenyl isocyanide (1.3 mmol, 0.173 g) was weighed into a separate 20 mL vial. The DMP-CN was quantitatively transferred with 3 × 1 mL portions of dry DCM into the vial containing the $[Co(PY5Me_2)(ACN)(PF_6)_2$ complex. Another 10 mL of dry DCM was added, and the mixture was stirred for 24 hours. The solvent was then removed by roto-evaporation outside the glovebox. The product was brought back into the glovebox and was washed with 3 × 2 mL portions of dry diethyl ether (yield: 0.782 g, 88.0%). Elemental analysis: found (calculated) for $Co(PY5Me_2)(DMP\text{-}CN)(PF_6)_2 \bullet CH_2Cl_2$, $C_{39}H_{36}Cl_2CoF_{12}N_6P_2$: C, 46.64(46.45); H, 3.47(3.60); N, 8.47(8.33).

[Co(PY5Me$_2$)(DMP-CN)](PF$_6$)$_3$ Synthesis

$[Co(PY5Me_2)(DMP\text{-}CN)](PF_6)_2$ (0.54 mmol, 0.500 g) was weighed into a 20 mL vial. $[TBPA](PF_6)$ (0.54 mmol, 0.339 g) was weighed into a separate 20 mL vial. The $[TBPA](PF_6)$ was quantitatively transferred with 3 × 2 mL portions of dry dichloromethane into the vial with $[Co(PY5Me_2)(DMP\text{-}CN)](PF_6)_2$. The dark red solution was then stirred, resulting in the precipitation of a yellow solid. After stirring for 2 hours the mixture was centrifuged at 3000 rpm for 5 minutes outside the glovebox. The solvent was then decanted and the solid was washed with

3 × 2 mL portions of dichloromethane with centrifugation between each wash at 3000 rpm for 5 minutes (yield: 0.354 g, 61.2%). ^{1}H NMR (500 MHz, acetonitrile-d3, 0.2 M DMP-CN) δ 9.77 – 9.65 (d, J = 6.23 4H), 8.48 (dd, J = 8.6, 7.3 Hz, 1H), 8.39 (d, J = 7.9 Hz, 2H), 8.30 – 8.21 (m, 8H), 7.78 (td, J = 6.4, 2.6 Hz, 4H), 7.58 (t, J = 7.7 Hz, 1H), 7.41 (d, J = 7.7 Hz, 2H), 2.94 (s, 6H), 2.25 (s, 6H). Elemental analysis: found (calculated) for $C_{38}H_{34}CoF_{18}N_6P_3$: C, 41.34(42.71); H, 3.14(3.21); N, 7.51(7.86).

DSSC Fabrication

TEC 15 FTO was cut into 1.5 cm × 2 cm pieces which were sonicated in soapy DI water for 15 minutes, followed by manual scrubbing of the FTO with Kimwipes. The FTO pieces were then sonicated in DI water for 10 minutes, rinsed with acetone and sonicated in isopropanol for 10 minutes. The FTO pieces were dried in room air then immersed in an aqueous 40 mM solution $TiCl_4$ solution for 30 minutes at 70 °C. The FTO pieces were immediately rinsed with 18 MΩ water and were annealed by heating from room temperature to 500 °C, and holding at 500 °C for 30 minutes. A 0.36 cm^2 area was doctor bladed with commercial 30 nm TiO_2 nanoparticle paste (DSL 30NRD) that was diluted with equal masses of α-terpinol and 10% ethyl cellulose by weight in ethanol. The transparent films were left to rest for 10 minutes and were then placed in a 100 °C oven for 15 minutes. The oven was then ramped to 325 °C for 5 minutes, 375 °C for 5 minutes, 450 °C for 5 minutes, and 500 °C for 15 minutes. After cooling to room temperature, a scattering layer was applied (PST-400C, JGC Catalysts) and annealed by the same method as the transparent layer. The 30 nm nanoparticle film thickness was measured to be 1 μm, and a total film thickness of 6.5 μm with the addition of the scattering layer . After cooling to room temperature, a second $TiCl_4$ treatment was performed as described above. When the anodes had cooled to 80 °C, they were soaked in a dye solution of 0.1 mM D35cpdt with 0.1 mM chenodeoxycholic acid in 1:1

acetonitrile:tert-butanol for 18 hours. After soaking, the anodes were rinsed with acetonitrile and were dried gently under a stream of nitrogen.

The PEDOT counter electrodes were prepared by electropolymerization in a solution of 0.01 M EDOT in 0.1 M SDS in 18 MΩ water.[20] A constant current of 8.3 mA for 300 seconds was applied to a 54 cm^2 piece of TEC 15 FTO with predrilled holes using an equal size piece of FTO as the counter electrode. The PEDOT electrode was then washed with DI water and acetonitrile before being dried under a gentle stream of nitrogen and cut into 1.5 cm by 2.0 cm pieces. The working and counter electrodes were sandwiched together with 25 μm surlyn films by placing them on a 140 °C hotplate and applying pressure with a hot iron. Contact to the TiO_2 electrode was made by scratching the edge of the electrode gently with sandpaper and applying silver epoxy and copper wire. The counter electrode was connected directly with silver epoxy and copper wire. The silver epoxy was dried in a 60 °C vacuum oven for 90 minutes and then the cells were filled with electrolyte through one of the two predrilled holes and were sealed with 25 μm surlyn backed by a glass coverslip and applied heat to seal. The electrolyte consisted of 0.15 M Co(II), 0.01 M Co(III) and 0.1 M $LiPF_6$ in dry acetonitrile. 0.2 M dimethyl phenyl isocyanide was also solvated in the $[Co(PY5Me_2)(DMP\text{-}CN)]^{3+/2+}$ electrolyte. Cells were measured approximately 18 hours after fabrication where they rested in ambient lighting. Ten dye-sensitized solar cells were measured for each electrolyte condition.

Instrumentation

ATIR spectra were collected in a JASCO FT/IR-6600 spectrometer under ambient air with 64 scans and 2 cm^{-1} resolution. NMR spectra were collected at room temperature on an Agilent DirectDrive2 500 MHz spectrometer and referenced to residual solvent signals. All NMR spectra were evaluated using the MestReNova software package features. All coupling constants are

apparent J values measured at the indicated field strengths in Hertz (s = singlet, d = doublet, t = triplet, q = quartet, dd = doublet of doublets, ddd = doublet of doublet of doublets, td = triplet of doublets, m = multiplet). Cyclic voltammograms were collected using a μAutolabIII potentiostat using a BASi glassy carbon working electrode, a fabricated platinum mesh counter electrode, and a fabricated 0.01 M $AgNO_3$, 0.1 M $TBAPF_6$ in acetonitrile $Ag/AgNO_3$ reference electrode. All measurements were also internally referenced to the ferrocenium/ferrocene couple by addition of ferrocene to the solution after measurements or measured in a separate solution of the same solvent and supporting electrolyte. Photoelectrochmical measurements were performed with a potentiostat (Autolab PGSTAT 128N) in combination with a xenon arc lamp. An AM 1.5 solar filter was used to simulate sunlight at 100 mW cm^{-2}, and the light intensity was calibrated with a certified reference cell system (Oriel Reference Solar Cell & Meter). A 400 nm long-pass filter was used to prevent direct excitation of the TiO_2 in all light measurements. A black mask with an open area of 0.12 cm^2 was applied on top of the cell active area. The solution potential of the devices was determined by immersing a platinum wire and the $Ag/AgNO_3$ electrode into the electrolyte used to fill the devices and measuring the potential between the electrodes. A monochromator (Horiba Jobin Yyon MicroHR) attached to the 450 W xenon arc light source was used for monochromatic light for IPCE measurements. The photon flux of the light incident on the samples was measured with a laser power meter (Nova II Ophir). IPCE measurements were made at 20 nm intervals between 400 and 800 nm at short circuit current. EIS measurements were measured with an Autolab PGSTAT 128N/FRA2 potentiostat/frequency response analyzer and all data plots were simulated with ZView software. Variable light intensity EIS measurements were made by using optical filters from Thorlabs (NEK01). Equivalent circuits used for EIS fitting can be found in the supporting information (Figure S11)). UV−vis spectra were measured with a

PerkinElmer Lambda 35 UV−vis spectrometer using 1 cm path length quartz cuvettes at 480 nm min^{-1}. CHN analysis were obtained at Midwest Microlab. For single crystal X-ray diffraction, single crystals were mounted on a nylon loop with paratone oil on a Bruker APEX-II CCD diffractometer. The crystals were kept at T = 173(2) K during data collection. Using Olex2 (Dolomanov et al., 2009), the structures were solved with the ShelXS (Sheldrick, 2008) structure solution program, using the Direct Methods solution method. The model was refined with version 2014/6 of XL (Sheldrick, 2008) using Least Squares minimization. All non-hydrogen atoms were refined anisotropically. Hydrogen atom positions were calculated geometrically and refined using the riding model.

Transient absorption spectroscopy

Transient absorption measurements were performed using a Vibrant 355 Nd:YAG/OPO (OPOTEK) tunable laser system (λ_ex = 550 nm). A probe pulse generated by a LP980 laser flash photolysis system (Edinburgh Instruments) monitored the decay of the oxidized dye population (λ_pr = 700 nm). Pulses were generated at a frequency of 1 Hz. A linear polarizer (Thorlabs) was used to limit the energy density to of the pump pulse to 0.3 mJ/cm^2. Samples were positioned at a 45° angle to both light sources using a homemade sample clamp fastened to a stationary stage. Raw signal was collected alongside fluorescence and probe background scans which were applied to the raw signal as corrections using LP900 software program (Edinburgh Instruments). The corrected scans were averaged 50 times for each run to improve S/N. 6 devices were fabricated for each of the four electrolyte conditions studied and the results obtained from fitting each individual spectrum were averaged. The data was fit using a bi-exponential using the Logger Pro software package. Samples were prepared in identical fashion as the electrodes described above, however a larger active area of 0.49 cm^2 comprised of a 6 μm thick film of 30 nm TiO_2 nanoparticles was

fabricated The devices were allowed to rest for 24 hours before being measured to allow for the devices to equilibrate. The inert electrolyte consisted of 0.1 M $LiPF_6$ in acetonitrile and the cobalt electrolytes consisted of 0.15 M Co(II), 0.10 M Co(III) and 0.1 M $LiPF_6$ in acetonitrile. The $[Co(PY5Me_2)(DMP\text{-}CN)](PF_6)_{3/2}$ electrolyte also had 0.2 M DMP-CN present.

Results and Discussion

The $[Co(PY5Me_2)(I)]I$ and $[Co(PY5Me_2)(ACN)](PF_6)_2$ complexes were synthesized as reported previously.[19] The bound acetonitrile of $[Co(PY5Me_2)(ACN)](PF_6)_2$ was readily substituted with 2,6-dimethylphenyl isocyanide (DMP-CN) using a moderate excess (1.5 equivalents) in the non-coordinating solvent dichloromethane. Oxidation of $[Co(PY5Me_2)(ACN)](PF_6)_2$ and $[Co(PY5Me_2)(DMP\text{-}CN)](PF_6)_2$ resulted in coordination of fluoride ions or nitrosonium biproducts when silver(I) hexafluorophosphate or nitrosonium hexafluorophosphate were used, respectively. The outer-sphere oxidant 4-bromotriphenylamine hexafluorophosphate $[TBPA](PF_6)$ was then used. The $[TBPA]^+$ oxidant was synthesized in dichloromethane from 1.00 equivalent of 4-bromotriphenylamine and 0.95 equivalents of nitrosonium hexafluorophosphate to insure nitrosonium was not present when using $[TBPA](PF_6)$ in the subsequent oxidation.[21] The oxidation of the Co(II) complexes occurred immediately upon addition of $[TBPA](PF_6)$ as indicated by the color change of the solution from dark blue to dark red. Both Co(III) complexes were readily purified of the oxidant by washing with dichloromethane to remove both oxidation states of the triphenylamine present.

Crystal structures were obtained for the $[Co(PY5Me_2)(DMP\text{-}CN)](PF_6)_2$, $[Co(PY5Me_2)(DMP\text{-}CN)](PF_6)_3$, $[Co(PY5Me_2)(ACN)](PF_6)_2$, and $[Co(PY5Me_2)(ACN)](PF_6)_3$ complexes. The $[Co(PY5Me_2)(DMP\text{-}CN)]^{2+}$ complex has shorter axial bonds between the Co(II) and the isocyanide ligand and central pyridine ligand, resulting in a distorted octahedral structure,

compared to the $[Co(PY5Me_2)(ACN)]^{2+}$ complex. The reduction in the degeneracy of the bonding and antibonding orbitals for the $[Co(PY5Me_2)(DMP\text{-}CN)](PF_6)_2$ complex is a result of being a low-spin Co(II) complex, which was confirmed by the Evan's method to measure the effective magnetic moment (μ_{eff}). This asymmetry is also present for the low-spin Co(II) complexes $[Co(PY5Me_2)(CN)](OTf)$ and $[Co(ttcn)_2](BF_4)_2$ reported previously.[16,22] Coordination of the strong-field isocyanide ligand to cobalt metal centers also results in a significant reduction of the metal to ligand bond distance changes upon oxidation compared to the acetonitrile bound complex. The average metal to ligand bond change for the $[Co(PY5Me_2)(DMP\text{-}CN)]^{3+/2+}$ couple is 0.082 Å which is close to half the change for the $[Co(PY5Me_2)(ACN)]^{3+/2+}$ couple at 0.156 Å. The reduction of the metal to ligand bond distance change upon oxidation significantly impacts the inner-sphere reorganization energy of the isocyanide redox couple.

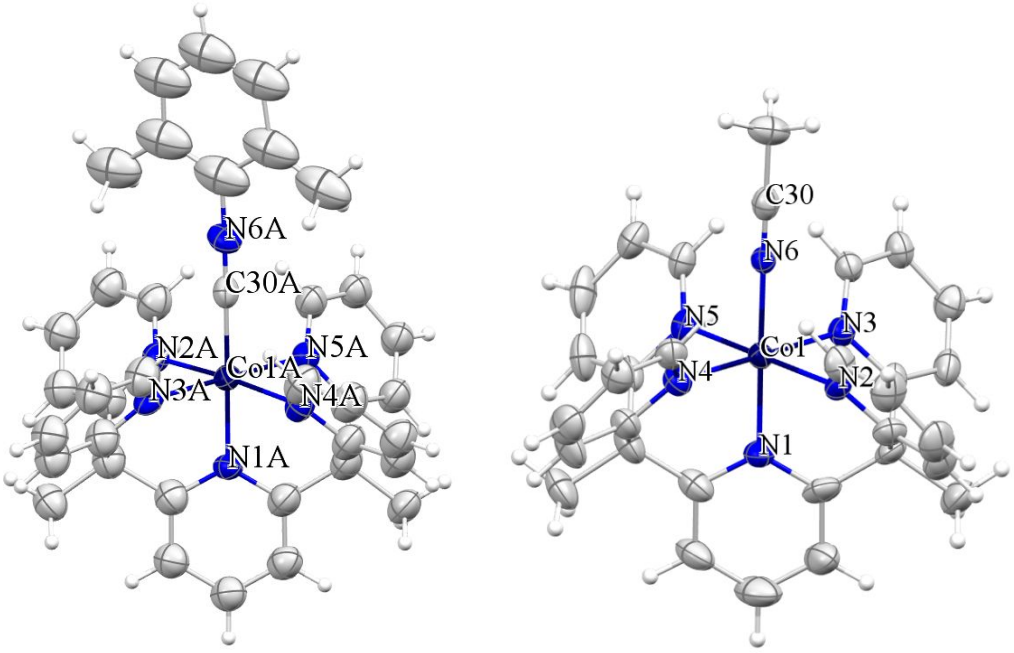

Figure 1: Structures of $[Co(PY5Me_2)(DMP\text{-}CN)](PF_6)_2$ (left) and $[Co(PY5Me_2)(ACN)](PF_6)_2$ (right).

Bond	$[Co(PY5Me_2)(DMP\text{-}CN)]^{2+}$	$[Co(PY5Me_2)(DMP\text{-}CN)]^{3+}$	$[Co(PY5Me_2)(ACN)]^{2+}$	$[Co(PY5Me_2)(ACN)]^{3+}$
Co-N1	1.969(4)	1.960(3)	2.094(3)	1.959(7)
Co-N2	2.123(5)	1.996(3)	2.137(3)	1.996(7)
Co-N3	2.060(5)	1.990(3)	2.133(3)	1.973(7)
Co-N4	2.138(5)	1.980(3)	2.130(3)	1.984(7)
Co-N5	2.078(4)	1.960(3	2.121(3)	1.982(7)
Co-C30	1.884(6)	1.878(4)	—	—
C30-N6	1.162(7)	1.135(5)	1.134(5)	1.116(10)
Co-N6	—	—	2.132(4)	1.917(6)

Table 1: Bond distances **(Å)** from single crystal X-ray diffraction data. $[Co(PY5Me_2)(DMP\text{-}CN)](PF_6)_2$ bond lengths are from structure A of the data set and $[Co(PY5Me_2)(ACN)](PF_6)_2$ bond lengths are from structure 1 of the data set.

In order to estimate the effect of the spin state on the inherent electron transfer barrier, the inner-sphere (λ_{in}), outer-sphere (λ_o) and total reorganization (λ) energies were calculated for each complex. Using symmetrical stretching frequencies of $\nu_{(Co(\mathrm{II})-N)}$ = 266 cm^{-1} from $[Co(bpy)_3](ClO_4)_2$ and $\nu_{(Co(\mathrm{III})-N)}$ = 378 cm^{-1} from $[Co(phen)_3](ClO_4)_3$, the force constants for each complex were estimated.[23,24] The effective force constant (f_{eff}) was then calculated and used with the change in each metal to ligand bond distance (Δd) of each complexs crystal structure to obtain the inner-sphere reorganization energy.[25]

$$f_1 = 4\pi^2 \nu^2_{Co(II)-N} \mu_{eff} \quad (1)$$

$$f_{eff} = \frac{2f_1 f_2}{f_1 + f_2} \quad (2)$$

$$\lambda_{in} = \frac{1}{2}\sum f_{eff} \Delta d^2 \quad (3)$$

The calculated inner-sphere reorganization energy of 2.76 eV for $[Co(bpy)_3]^{3+/2+}$ is in good agreement with the value of 2.63 eV derived from the self-exchange rate constant.[13] The $[Co(PY5Me_2)(ACN)]^{3+/2+}$ λ_{in} is reduced significantly to 1.74 eV despite also being a high-spin Co(II) complex. Similar redox couples, $[Co(PY5Me_2)(NMBI)]^{3+/2+}$ and $[Co(PY5Me_2)(TBP)]^{3+/2+}$, display similar average changes in bond length (Δd = 0.15 Å), which is attributed to the constrained nature of the $PY5Me_2$ ligand influencing structural changes.[15] The $[Co(PY5Me_2)(DMP\text{-}CN)]^{3+/2+}$ couple displays even larger reductions in the inner-sphere reorganization energy, with a calculated value of0.77 eV. The $[Co(PY5Me_2)(DMP\text{-}CN)](PF_6)_2$ complex has a low-spin d^7 electronic structure which reduces the electronic rearrangement, with a loss of only one electron from an anti-bonding $d_{x^2-y^2}$ orbital during the oxidation, compared to removal of one electron and pairing of another for high-spin d^7 complexes. We note that one bond of each of the $[Co(PY5Me_2)(DMP\text{-}CN)]^{3+/2+}$ complexes are Co-C bonds, and the force constants are taken from Co-N bond frequencies for the analysis above. This assumption does not affect the result of the calculation since the Co(II)-C bond and the Co(III)-C bond are statistically the same, and thus Δd = 0 in the calculation for those bonds.[26]

The outer-sphere reorganization energy was also determined from the crystal-structure data. The radius was averaged for each cobalt to exterior hydrogen, of the ligands, of the $[Co(PY5Me_2)(ACN)](PF_6)_{3/2}$ and the $[Co(PY5Me_2)(DMP\text{-}CN)](PF_6)_{3/2}$ couples. Using the dielectric constant (ε_0 = 36.64 F cm^{-1}) and refractive index of acetonitrile (n_{sol} = 1.3442), the

radius of each reactant (a_1 and a_2) and center to center distance (R), the outer-sphere reorganization energy was calculated according to equation 4.[27,28]

$$\lambda_o = \frac{\Delta e^2}{4\pi\varepsilon_{vac}}\left(\frac{1}{2a_1} + \frac{1}{2a_2} - \frac{1}{R}\right)\left(\frac{1}{{n_{sol}}^2} - \frac{1}{\varepsilon_0}\right) \quad (4)$$

Comparing the outer-sphere reorganization energies, the largest radius $[Co(bpy)_3]^{3+/2+}$ has the smallest outer-sphere reorganization energy and increases marginally as the radius decreases for $[Co(PY5Me_2)(ACN)]^{3+/2+}$ and $[Co(PY5Me_2)(DMP\text{-}CN)]^{3+/2+}$. From the sum of the outer-sphere and inner-sphere reorganization energies, the total reorganization energy was calculated for each complex. The total reorganization energy is dominated by the inner-sphere reorganization energy for each complex due to the large ligand to metal bond distance changes upon electron transfer. For the $[Co(PY5Me_2)(DMP\text{-}CN)]^{3+/2+}$ couple, both the coordination of the $PY5Me_2$ and DMP-CN ligand results in the largest reduction in reorganization energy. Comparing the $[Co(PY5Me_2)(DMP\text{-}CN)]^{3+/2+}$ couple to $[Co(bpy)_3]^{3+/2+}$, the total reorganization energy is almost 2 eV lower, 1.42 eV compared to 3.37 eV. According to Marcus theory, the $[CoPY5Me_2)(DMP\text{-}CN)]^{3+/2+}$ couple will have a lower barrier for both regeneration and recombination compared to $[Co(bpy)_3]^{3+/2+}$ and $[Co(PY5Me_2)(ACN)]^{3+/2+}$.

Table 2: Redox potential, effective magnetic moment for Co(II) complexes, complex radius, average bond distance change, inner-sphere, outer-sphere, and total reorganization energy.

	$E_{1/2}$ *vs.* Fc^+/Fc (V)	μ_{eff} (μ_b)	*R* (Å)	Δd (Å)	λ_{in} (eV)	λ_o (eV)	λ (eV)
$[Co(bpy)_3]^{3+/2+}$	-0.066	~ 4.6 [29]	6.5 [30]	0.198 [31,32]	2.76	0.62	3.37
$[Co(PY5Me_2)(ACN)]^{3+/2+}$	0.165	4.25 ± 0.01	5.6	0.156	1.74	0.71	2.45
$[Co(PY5Me_2)(DMP\text{-}CN)]^{3+/2+}$	0.098	2.08 ± 0.02	6.1	0.082	0.77	0.66	1.42

For both oxidation states of the $[Co(PY5Me_2)(DMP\text{-}CN)]^{3+/2+}$ complexes, the bound DMP-CN was found to be labile in neat acetonitrile. When the $[Co(PY5Me_2)(DMP\text{-}CN)](PF_6)_2$ complex is introduced into deuterated acetonitrile for ^1H NMR studies, immediately after solvation the spectrum consists of a mixture of $[Co(PY5Me_2)(ACN)](PF_6)_2$ and $[Co(PY5Me_2)(DMP\text{-}CN)](PF_6)_2$, indicating rapid ligand dissociation without the excess isocyanide (Figure 2a). As the DMP-CN concentration is increased the downfield signals between 25 ppm to 95 ppm associated with the $[Co(PY5Me_2)(ACN)(PF_6)_2$ complex decrease while the peaks lower than 30 ppm increase, which is assigned to the $[Co(PY5Me_2)(DMP\text{-}CN)](PF_6)_2$ complex. To confirm the peaks assigned to the $[Co(PY5Me_2)(DMP\text{-}CN)](PF_6)_2$ complex, ^1H NMR was also matched in the non-coordinating solvent deuterated dichloromethane to insure no ligand displacement. Therefore, to maintain the $[Co(PY5Me_2)(DMP\text{-}CN)]^{3+/2+}$ couple, 0.2 M DMP-CN was used to eliminate any significant contributions of the $[Co(PY5Me_2)(ACN)]^{3+/2+}$ couple for all measurements in acetonitrile.

The effect of substitution of DMP-CN by ACN was also measured by differential pulse voltammetry. In the differential pulse voltammetry experiments, the $[Co(PY5Me_2)(DMP\text{-}CN)]^{3+/2+}$ couple has a broad peak when dissolved in ACN with supporting electrolyte. This is likely due to the solution having a mixture of both the $[Co(PY5Me_2)(DMP\text{-}CN)]^{3+/2+}$ and the $[Co(PY5Me_2)(ACN)]^{3+/2+}$ couple present. Upon addition of DMP-CN to the electrolyte, the peak maximum shifts negative until approximately 0.1 M of DMP-CN ligand was added and then the potential remains constant (Figure 2b). Comparing the redox potentials obtained by cyclic voltammetry, the $[Co(PY5Me_2)(DMP\text{-}CN)]^{3+/2+}$ couple is shifted 67 mV negative of the precursor $[Co(PY5Me_2)(ACN)]^{3+/2+}$ couple due to the donating nature of the DMP-CN ligand and lies 164 mV positive of the $[Co(bpy)_3]^{3+/2+}$ couple. The $[Co(PY5Me_2)(DMP\text{-}CN)](PF_6)_2$ complex was

found to be reversible at a glassy carbon electrode and from the scan rate dependence a diffusion coefficient of 2.8 ± 0.1 × 10^{-6} cm^2 s^{-1} was obtained which is similar to that determined previously for $[Co(bpy)_3]^{2+}$ (Figure S4).[33,34]

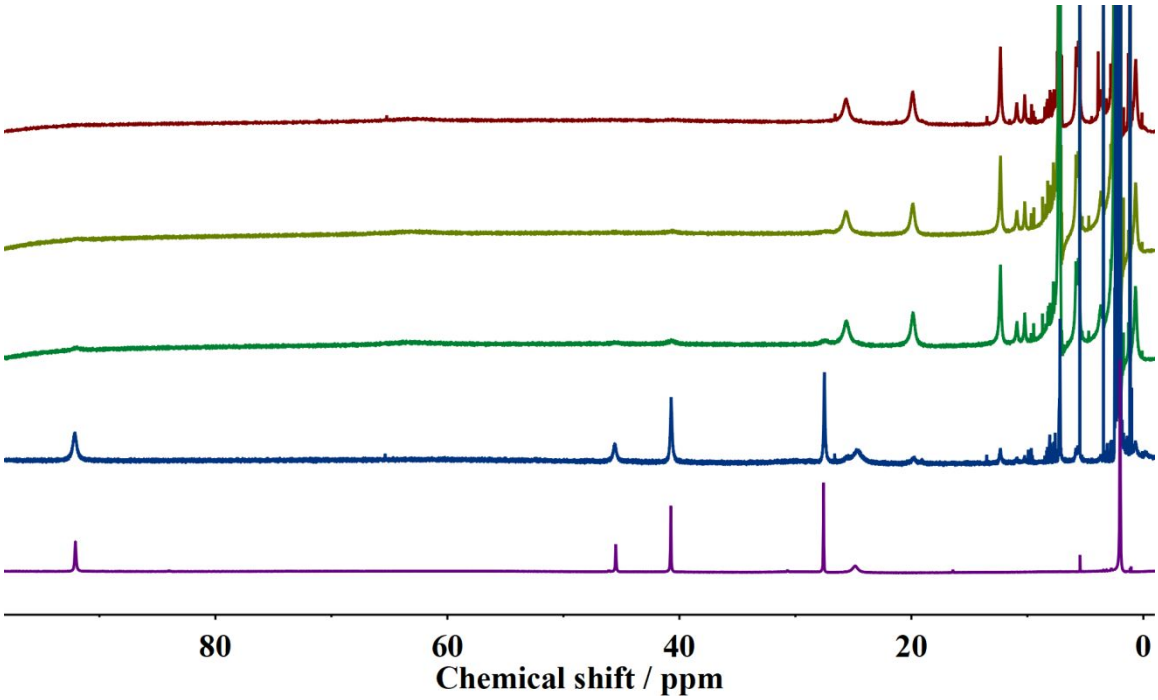

(a)

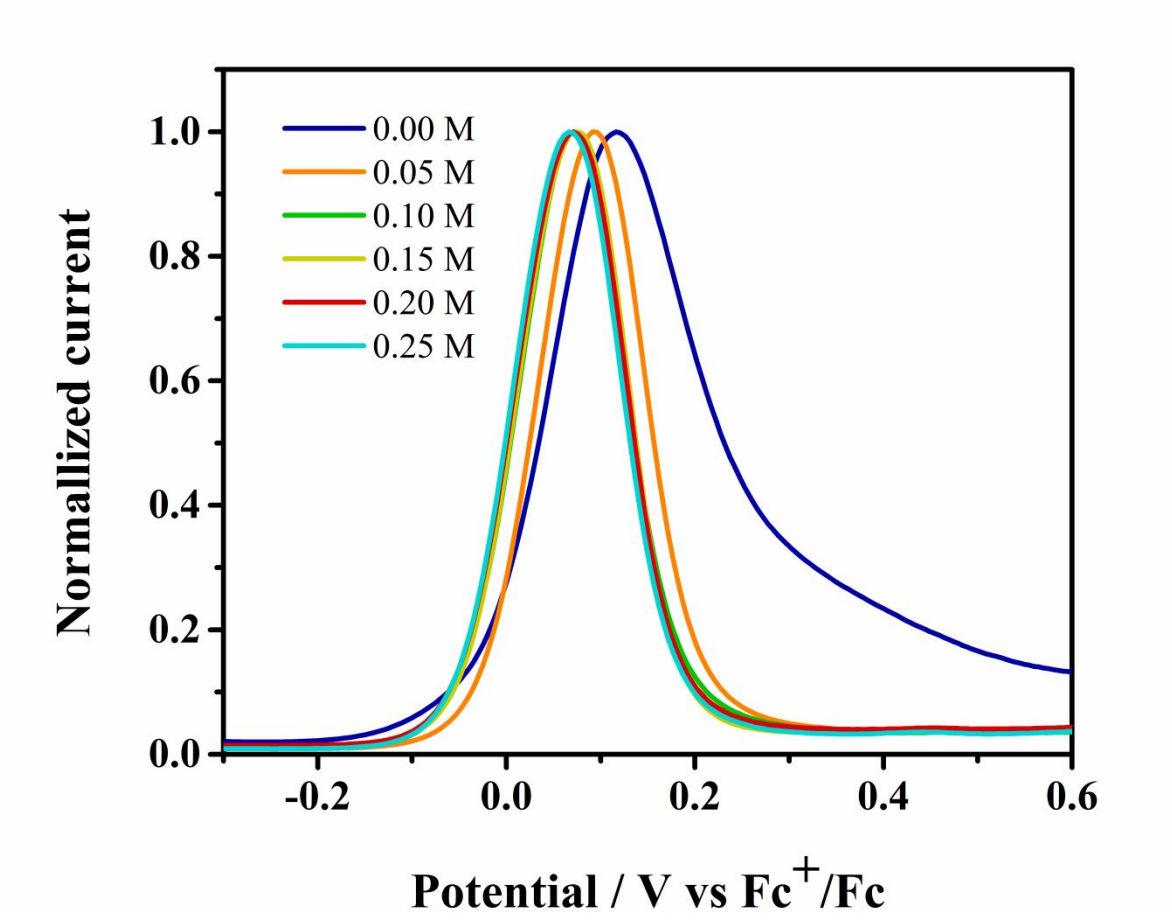

(b)

Figure 2: (a) ^{1}H NMR spectra of 15 mM [Co(PY5Me$_2$)(DMP-CN)(PF$_6$)$_2$ in acetonitrile with increasing concentration of DMP-CN: [Co(PY5Me$_2$)(ACN)](PF$_6$)$_2$ complex for reference (violet), 0.00 M DMP-CN (blue), 0.10 M DMP-CN (green), 0.15 M DMP-CN (yellow), and 0.20 M DMPCN (red). (b) Differential pulse voltammetry results of 5 mM [Co(PY5Me$_2$)(DMP-CN)](PF$_6$)$_2$ in acetonitrile with 100 mM TBAPF$_6$ and increasing concentrations of DMP-CN.

Dye-sensitized solar cells were fabricated using [Co(PY5Me$_2$)(DMP-CN)]$^{3+/2+}$, [Co(bpy)$_3$]$^{3+/2+}$ and [Co(PY5Me$_2$)(ACN)]$^{3+/2+}$ as redox shuttles. The [Co(bpy)]$^{3+/2+}$ and [Co(PY5Me$_2$)(DMP-CN)]$^{3+/2+}$ redox shuttles produce nominally the same current density (*J*) *vs*. applied voltage (*V*) behavior under simulated AM 1.5 illumination, and therefore power conversion efficiencies, despite the large differences in reorganization energy (Table 3). Interestingly, the [Co(PY5Me$_2$)(ACN)]$^{3+/2+}$ shuttle performed significantly worse than either [Co(bpy)]$^{3+/2+}$ or [Co(PY5Me$_2$)(DMP-CN)]$^{3+/2+}$, despite a reorganization energy value in between

the two. Some of the *J-V* behavior must therefore be attributed to differences in solution potential (E_{sol}), which determines the driving forces for the forward (dye regeneration) and reverse (recombination) reactions. The $[Co(PY5Me_2)(DMP\text{-}CN)]^{3+/2+}$ couple has a larger driving force for recombination and a smaller driving force for regeneration compared to the $[Co(bpy)]^{3+/2+}$ couple. Therefore, dye regeneration and recombination kinetics were investigated in detail below as a function of redox shuttle. We note the photocurrents obtained by integrating IPCE curves substantiate the short circuit photocurrent density, J_{sc}, determined by the *J-V* curves.

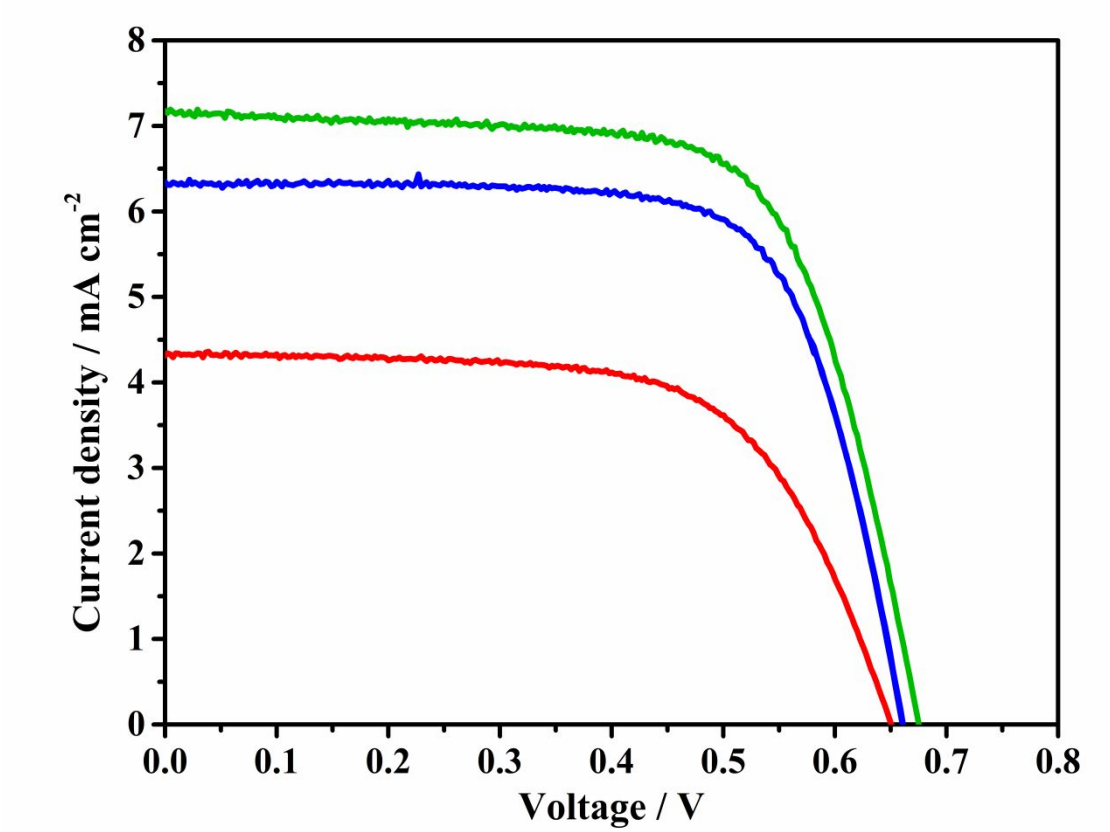

(a)

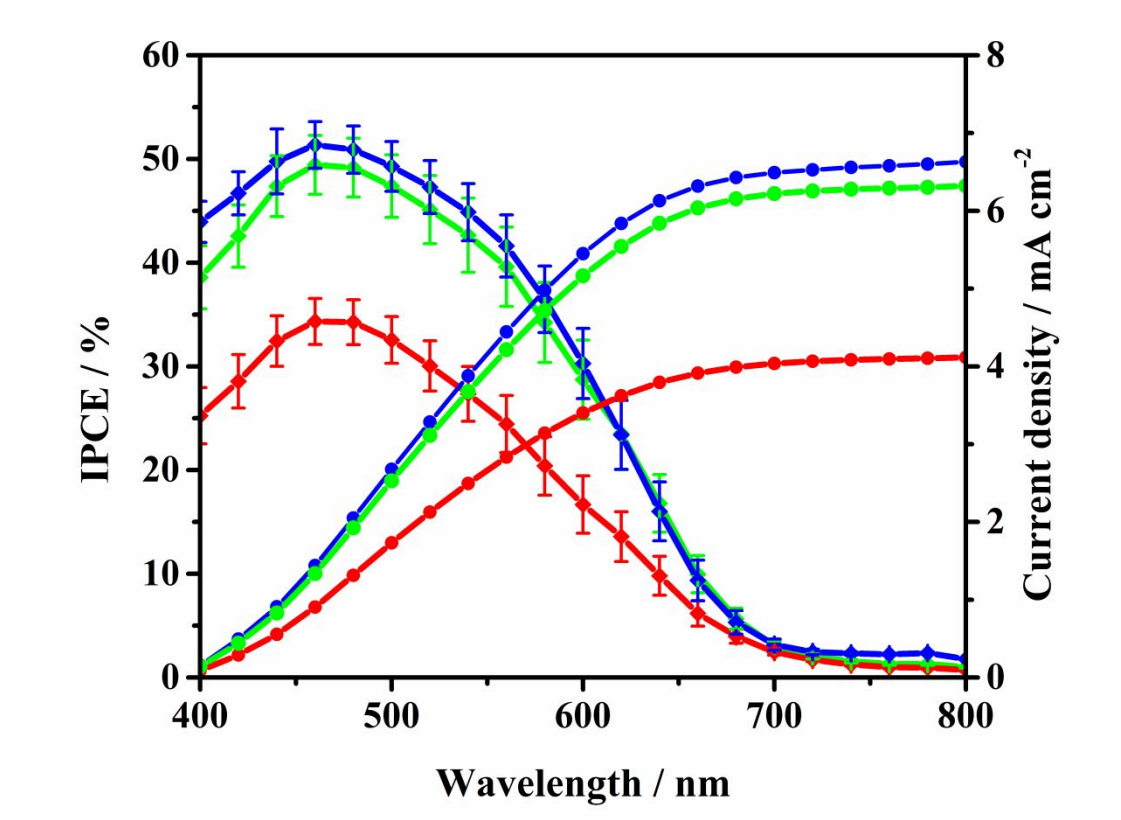

(b)

Figure 3: (a) Plots of current density *vs*. applied voltage curves under 100 mW cm^{-2} illumination for the [Co(PY5Me$_2$)(DMP-CN)]$^{3+/2+}$ (green), [Co(bpy)$_3$]$^{3+/2+}$ (blue) and [Co(PY5Me$_2$)(ACN)]$^{3+/2+}$ (red) electrolytes. (b) Incident photon-to-current conversion efficiency (diamonds) of [Co(PY5Me$_2$)(DMP-CN)]$^{3+/2+}$ (green), of [Co(bpy)$_3$]$^{3+/2+}$ (blue) and of [Co(PY5Me$_2$)(ACN)]$^{3+/2+}$ (red) electrolytes using monochromatic light and the integrated J_{sc} (circles).

In order to compare the kinetics and efficiency of dye regeneration reaction as a function of redox shuttle, nano-second transient absorption spectroscopy (TAS) measurements were performed. The D35cpdt dye was excited by a pump beam at 550 nm and after the approximately pico-second time scale associated with electron injection to the TiO_2, the oxidized dye was monitored at 700 nm.[35] Due to the complex nature of the kinetic traces, the data could not be fit to a single stretched exponential so a bi-exponential was used to obtain each time constant of the decay in accord with prior analyses.[36,37]

$$\Delta A(t) = \Delta A_0 + A_1 \exp^{-tk_1} + A_2 exp^{-tk_2} \quad (5)$$

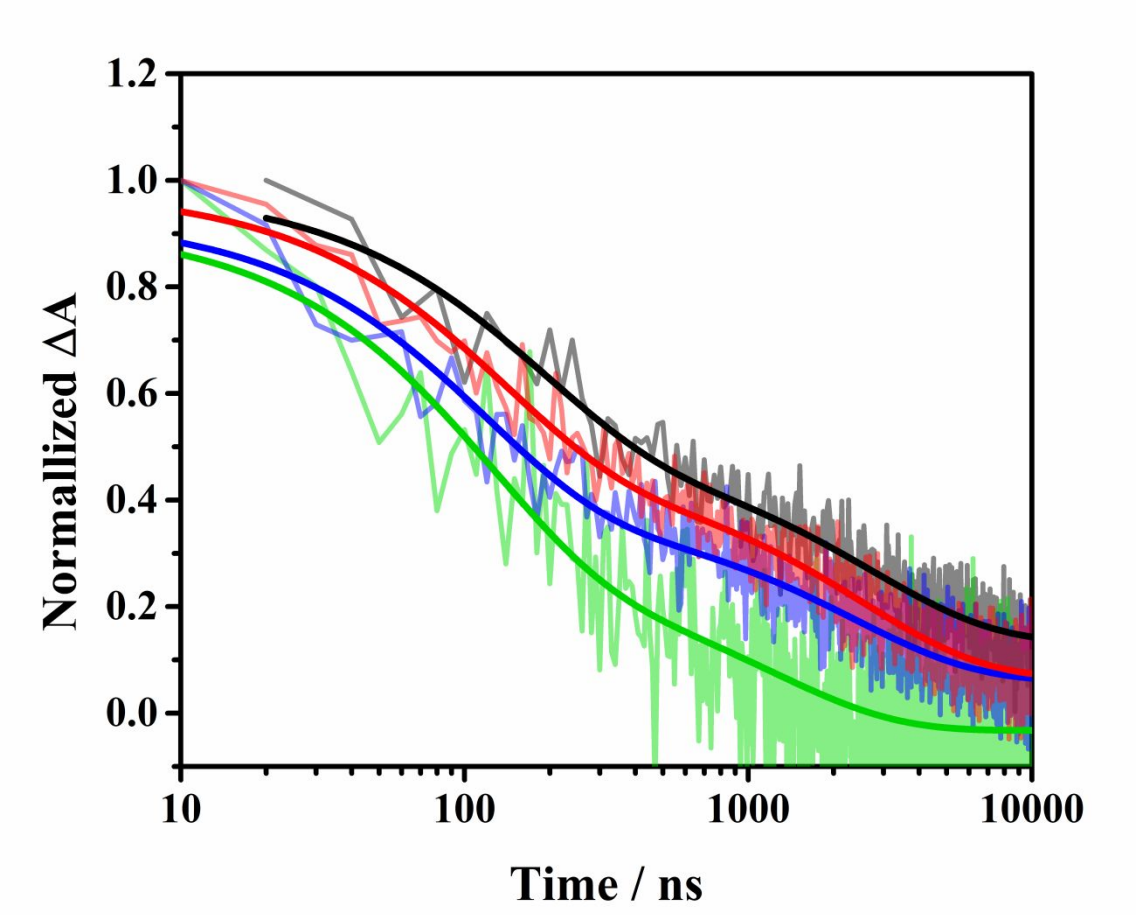

Figure 4: Transient absorption traces observed at 700 nm of the oxidized sensitizer with $[Co(PY5Me_2)(DMP\text{-}CN)]^{3+/2+}$ (green), $[Co(bpy)_3]^{3+/2+}$ (blue), $[Co(PY5Me_2)(ACN)]^{3+/2+}$ (red) and inert (black) with fits as solid lines. Electrolytes were the same composition as full DSSC electrolytes. Inert consisted of 0.1 M $LiPF_6$ in acetonitrile.

In equation 5, ΔA_0 is the change in absorbance at time zero, A_1 and A_2 are the pre-exponential factors for the contribution of each process and k_1 and k_2 are the observed rate constants of each process. From the results of fitting equation 5 to the decay curves displayed in Figure 4, the regeneration efficiency can be estimated by solving for the time at $\Delta A = 0.5$, to obtain the $t_{1/2}$ for both recombination and regeneration. The recombination halftime ($t_{1/2rec}$) was obtained without the presence of a redox couple and the regeneration halftimes ($t_{1/2reg}$) were obtained in the presence of each redox couple. The $t_{1/2rec}$ was found to be 344 ± 57 ns, which is somewhat faster than values

found within the literature.[36,38] It has been previously shown that the time-scale of recombination to the D35cpdt dye is influenced strongly by the pump light intensity (i.e. initial TiO_2 electron concentration).[39] It was found that the $t_{1/2rec}$ spanned three orders of magnitude by varying the pump light intensity; therefore its absolute value is dependent on the experimental conditions of the device and the transient absorption setup. However, the redox couple's $t_{1/2reg}$ is less dependent on light intensity which allows for a sound comparison of the relative ability of each redox shuttle to regenerate the D35cpdt dye. From the ratio of the $t_{1/2rec}$ and the $t_{1/2reg}$, the regeneration efficiency (Φ_{reg}) can be estimated for each redox shuttle according to:[40]

$$\Phi_{reg} = \frac{k_{reg}}{k_{reg} + k_{rec}} = 1 - \frac{t_{1/2reg}}{t_{1/2rec}} \quad (6)$$

Introduction of each redox couple accelerates the decay of the oxidized sensitizer, as expected. The $[Co(PY5Me_2)(DMP\text{-}CN)]^{3+/2+}$ shuttle displays the fastest regeneration kinetics and associated regeneration efficiency (Table 3). Specifically, the D35cpdt regeneration is twice as fast with $[Co(PY5Me_2)(DMP\text{-}CN)]^{2+}$ compared to $[Co(bpy)_3]^{2+}$, despite a 160 mV smaller driving force for the reaction. The faster regeneration can be attributed to the reduced inner-sphere reorganization energy.[41,40] We note that the regeneration efficiency is lower than what is typically reported for the $[Co(bpy)_3]^{3+/2+}$ couple, which is partly due to using a lower concentration of the Co(II) complexes due to solubility limitation of the $[Co(PY5Me_2)]^{3+/2+}$ couples, 0.15 M relative to 0.20-0.25 M seen in the literature.[37,40,42] In addition, as noted above, the efficiency is determined by the recombination kinetics, which is highly variable by system and laser power intensity, which makes the trend, or relative values, more meaningful than the absolute efficiencies determined. The $[Co(PY5Me_2)(ACN)]^{3+/2+}$ couple has an even smaller driving force for regeneration than

$[Co(PY5Me_2)(DMP\text{-}CN)]^{2+}$ and larger reorganization energy, which explains the slow kinetics, poor regeneration efficiency and photocurrent density measured with the redox shuttle.

To illustrate a clearer description of the influence of the reorganization energy and driving force on regeneration process, the dye regeneration ($k_{et,reg}$) can be modeled and compared using Marcus theory:[28]

$$k_{et,reg} \propto e^{-(\Delta G_{reg} + \lambda_{reg})^2/4\lambda_{reg}k_B T} \quad (7)$$

Since the pre-exponential term (e.g. coupling) is expected to be nominally constant for the redox couple-dye pairs, relative rate constants can be estimated through comparisons of the nuclear terms. The driving force of regeneration (ΔG_{reg}) is taken from the difference of the redox potential of the redox shuttles and the redox potential of the dye D35cpdt (0.45 V *vs.* Fc^+/Fc) measured previously on TiO_2.[13] The reorganization energy of the regeneration event (λ_{reg}) is the average of each redox couples reorganization energy with the sensitizers reorganization energy. We are not aware of the reorganization energy being measured previously for D35cdpt but similar triarylamine sensitizers reorganization energies have been estimated computationally, which provides a value of 0.95 eV that we use here.[43] From the calculations of the exponential term of the Marcus equation, the $[Co(PY5Me_2)(DMP\text{-}CN)]^{3+/2+}$ couple is expected to have the fastest regeneration kinetics, while $[Co(bpy)_3]^{3+/2+}$ and $[Co(PY5Me_2)(ACN)]^{3+/2+}$ have nominally the same rate of regeneration. The regeneration efficiencies compared with the regeneration terms have a discrepancy between $[Co(PY5Me_2)(DMP\text{-}CN)]^{3+/2+}$ and $[Co(bpy)_3]^{3+/2+}$,where there is only a two-fold difference in regeneration halftime and a three order of magnitude difference in the calculated exponential term. This is likely due to an overestimation of the reorganization energy of $[Co(bpy)_3]^{3+/2+}$ when comparing the reorganization energy determined from the crystal

structures compared to that measured by self-exchange previously.[13,30] This would also explain Marcus theory's prediction of $[Co(bpy)_3]^{3+/2+}$ having a slower regeneration rate than $[Co(PY5Me_2)(ACN)]^{3+/2+}$, while the halftime for $[Co(bpy)_3]^{3+/2+}$ regeneration is faster. If the total reorganization energy values from the self-exchange rate constant of 2.64 eV and 3.21 eV were used to calculate the exponential term, the term would increase to 1.4×10^{-4} and 1.1×10^{-5}, respectively, making for greater agreement of the halftimes of regeneration and Marcus theory.

Table 3: Summarized average of each performance parameter for $[Co(bpy)_3]^{3+/2+}$, $[Co(PY5Me_2)(DMP\text{-}CN)]^{3+/2+}$ and $[Co(PY5Me_2)(ACN)]^{3+/2+}$ electrolytes used in dye-sensitized solar cells.

	$[Co(bpy)_3]^{3+/2+}$	$[Co(PY5Me_2)(DMP\text{-}CN]^{3+/2+}$	$[Co(PY5Me_2)(ACN)]^{3+/2+}$
E_{sol} *vs.* Fc^+/Fc (V)[a]	-0.156	0.044	0.084
V_{oc} (V)	0.66 ± 0.03	0.67 ± 0.02	0.64 ± 0.02
J_{sc} (mA cm^{-2})	6.6 ± 0.5	7.2 ± 0.5	4.3 ± 0.3
IPCE (mA cm^{-2})	6.63	6.31	4.11
FF	0.68 ± 0.03	0.69 ± 0.03	0.65 ± 0.02
η (%)	3.0 ± 0.2	3.4 ± 0.2	1.8 ± 0.2
$t_{1/2reg}$ (ns)	152 ± 30	86 ± 22	248 ± 40
Φ_{reg}	0.57 ± 0.09	0.75 ± 0.06	0.28 ± 0.11
ΔG_{reg} (eV)	0.52	0.35	0.29
λ_{reg} (eV)	2.16	1.19	1.72
$e^{-(\Delta G_{reg} + \lambda_{reg})^2/4\lambda_{reg}k_BT}$	5.04×10^{-6}	3.3×10^{-3}	8.2×10^{-6}

[a] Solution potential of electrolytes used to fill devices were measured with a platinum wire working electrode, platinum mesh counter electrode and fabricated $Ag/AgNO_3$ reference electrode measured to be -0.077 V *vs.* Fc^+/Fc.

Since the $[Co(PY5Me_2)(DMP\text{-}CN)]^{3+/2+}$ shuttle produces similar *J-V* behavior as the $[Co(bpy)_3]^{3+/2+}$ shuttle, despite more efficient dye regeneration and more positive solution potential enabling a larger V_{oc}, the recombination to $[Co(PY5Me_2)(DMP\text{-}CN)]^{3+}$ must be faster to offset these advantages. To evaluate recombination at the photoanode / electrolyte interface, photoelectrochemical impedance spectroscopy (PEIS) measurements were performed to compare electron recombination resistances, which are inversely proportional to recombination rates, at a given electron occupance.[44] Measurements were performed at open circuit to maintain constant Fermi levels ($E_{F,n}$) throughout the TiO_2 film, and the light intensity was varied to control the electron population, which is reflected in the chemical capacitance (C_μ) obtained from fitting the data to an equivalent circuit (Figures S10 and S11). Since the solution potentials are different for each electrolyte and the V_{oc} is the difference between solution (reference) potential and the $E_{F,n}$ of TiO_2, a correction needs to be introduced to compare recombination at the same $E_{F,n}$. The chemical capacitance provides quantitative information about the electron occupancy of TiO_2 at a given $E_{F,n}$, assuming a fixed conduction band potential, $E_{c,}$[45] according to:

$$C_\mu = L(1-p)\alpha\frac{q^2 N_t}{k_B T}\exp\left(\alpha\frac{(E_{redox}-E_c)}{k_B T}\right)\exp\left(\alpha\frac{qV_{oc}}{k_B T}\right) \quad (10)$$

where L is the film thickness, p is the porosity of TiO_2 film, q is the electron charge, k_B is Boltzmann's constant, T is the temperature, N_t is the total number of trap states below the conduction band, and α is the exponential electron trap distribution parameters.[46]

We note that the base DMP-CN has been added to the $[Co(PY5Me_2)(DMP\text{-}CN)]^{3+/2+}$ electrolyte, which can affect the band edge potential and lead to problems in comparing recombination rates.

Inspection of the chemical capacitance as a function of the applied potential (corrected for differences in solution potential) shows that the trend is not affected by the electrolyte, indicating that there is no detectable shift in band position for each electrolyte composition (Figure S12).

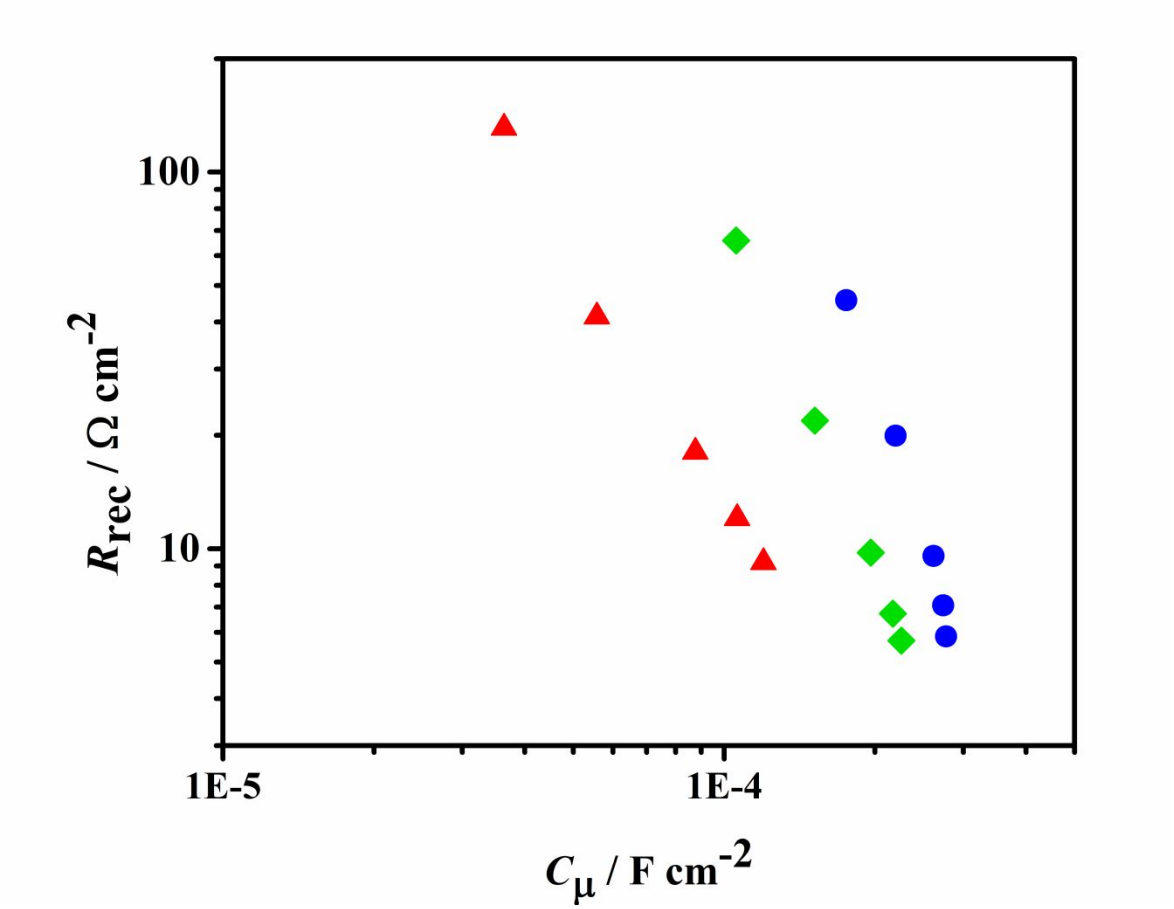

Figure 5: R_{rec} as a function of C_μ to compare at the same electron density (n) from results of the PEIS analysis of DSSCs at various light intensity conditions (100, 80, 50, 25 and 10 mW cm^{-2}) with $[Co(PY5Me2)(DMP\text{-}CN)]^{3+/2+}$ (green diamonds), $[Co(bpy)_3]^{3+/2+}$ (blue circles) and $[Co(PY5Me_2)(ACN)]^{3+/2+}$ (red triangles).

Figure 5 shows the extracted recombination resistance (R_{rec}) with respect to the capacitance by modulation of the light intensity, for the $[Co(PY5Me_2)(DMP\text{-}CN)]^{3+/2+}$, $[Co(bpy)_3]^{3+/2+}$ and $[Co(PY5Me_2)(ACN)]^{3+/2+}$ redox shuttles. The R_{rec} increases in the order of $[Co(PY5Me_2)(ACN)]^{3+/2+}$, $[Co(PY5Me_2)(DMP\text{-}CN)]^{3+/2+}$ and $[Co(bpy)_3]^{3+/2+}$ at a given C_μ which

means the recombination rate constants decrease in the same order. Given the potential of the TiO_2 conduction band measured previously in acetonitrile with lithium supporting electrolyte (0.8 V *vs.* Ag/AgCl) and the redox potentials of each redox couple, the driving force for recombination (ΔG_{rec}) can be estimated for each couple.[47] The outer-sphere reorganization energy can also be calculated for the TiO_2 (λ_{o,TiO_2}) and redox couple electron transfer as described previously.[13] Values are provided in Table 4. Relative to the other redox couples, $[Co(bpy)_3]^{3+/2+}$ has the slowest rate of recombination, which matches predictions made by Marcus theory given the largest reorganization energy and smallest driving force for recombination and being well within the Marcus normal region. However, comparisons of the $[Co(PY5Me_2)(ACN)]^{3+/2+}$ and $[Co(PY5Me_2)(DMP\text{-}CN)]^{3+/2+}$ redox shuttles are not as straightforward. While $[Co(PY5Me_2)(DMP\text{-}CN)]^{3+/2+}$ has a smaller reorganization energy and driving force for recombination relative to $[Co(PY5Me_2)(ACN)]^{3+/2+}$, they are both close to optimal exoergicity; $[Co(PY5Me_2)(ACN)]^{3+/2+}$ is expected to be in the normal region and $[Co(PY5Me_2)(DMP\text{-}CN)]^{3+/2+}$ is expected to be in the inverted region, and thus have similar rate constants for electron transfer from the conduction band. This analysis ignores contributions from sub-bandgap states, however, which may be significant and different for the two redox shuttles.[47] Another possible reason for the discrepancy between the recombination resistance measured and the trend expected from Marcus theory may be the excess DMP-CN ligand which is present in the $[Co(PY5Me_2)(DMP\text{-}CN)]^{3+/2+}$ electrolyte. The excess DMP-CN ligand may block recombination by coupling to TiO_2 states or sterically hindering charge transfer, analogous to 4-tert-butylpyridine.[48,49]

Table 4: Outer-sphere reorganization energy of TiO_2 and electrolyte interface λ_{o,TiO_2}, total reorganization energy of recombination event λ_{ET} and driving force for recombination from TiO_2 band to redox couple ΔG_{rec}.

	$[Co(bpy)_3]^{+3/+2}$	$[Co(PY5Me_2)(DMP\text{-}CN]^{+3/+2}$	$[Co(PY5Me_2)(ACN)]^{+3/+2}$
$\boldsymbol{\lambda_{o,TiO_2}}$ **(eV)**	0.531	0.561	0.608
$\boldsymbol{\lambda_{rec}}$ **(eV)**	1.909	0.947	1.504
$\boldsymbol{\Delta G_{rec}}$ **(eV)**	1.091	1.255	1.322

Conclusions

Utilizing the strong-field ligand 2,6-dimethylphenyl isocyanide in combination with the $Co(PY5Me_2)$ framework has resulted in a low-spin Co(II) redox couple with improved regeneration kinetics over $[Co(bpy)_3]^{2+}$, while utilizing 160 mV less driving force. Utilizing this redox couple with a more positive potential should have resulted in a larger open-circuit voltage, however the recombination rate also increased for $[Co(PY5Me_2)(DMP\text{-}CN)]^{3+}$ compared to $[Co(bpy)_3]^{3+}$ which offset the possible gains. $[Co(PY5Me_2)(DMP\text{-}CN)]^{3+/2+}$ displayed promising performance with a power conversion efficiency similar to $[Co(bpy)_3]^{3+/2+}$, however the performance has limited gains with the large recombination losses present. These results and analysis agree with our previous reports using the redox couple $[Co(ttcn)_2]^{3+/2+}$. Such attempts to make gains by lowering the reorganization energy, and thus reduce the energy penalty required to achieve efficient dye regeneration, has minimal benefits with large driving forces for TiO_2/electrolyte recombination ($\geq$ 1 eV).[13] The significant advantage of $[Co(PY5Me_2)(DMP\text{-}CN)]^{3+/2+}$ compared to $[Co(ttcn)_2]^{3+/2+}$, however, is that in principle the ligand can be modified with electron donating/withdrawing groups to modulate the redox potential (thus relative driving forces)

and thereby fully optimize devices with such low-spin cobalt redox systems. In order to capitalize on these low-spin cobalt redox shuttles, more negative redox potentials are needed. Although a sacrifice in V_{oc} will be made, this will be compensated by reduced recombination and broader light absorption with sensitizers that absorb deeper into the red.[50] Work is in progress in our lab to test this hypothesis.

Conflicts of interest

There are no conflicts to declare.

Acknowledgement

This work was supported by the Chemical Sciences, Geosciences, and Biosciences Division, Office of Basic Energy Sciences, Office of Science, the U.S. Department of Energy Grant No. DE-SC0017342.

References

(1) Kakiage, K.; Aoyama, Y.; Yano, T.; Oya, K.; Fujisawa, J. I.; Hanaya, M. Highly-Efficient Dye-Sensitized Solar Cells with Collaborative Sensitization by Silyl-Anchor and Carboxy-Anchor Dyes. *Chem. Commun.* **2015**, *51* (88), 15894–15897.

(2) Zakeeruddin, S. M.; Chang, S.-N.; Yella, A.; Hsieh, C.-H.; Mai, C.-L.; Grätzel, M.; Yeh, C.-Y. Molecular Engineering of Push-Pull Porphyrin Dyes for Highly Efficient Dye-Sensitized Solar Cells: The Role of Benzene Spacers. *Angew. Chemie Int. Ed.* **2014**, *53* (11), 2973–2977.

(3) Humphry-Baker, R.; Rothlisberger, U.; Nazeeruddin, M. K.; Yella, A.; Ashari-Astani, N.; Grätzel, M.; Tavernelli, I.; Gao, P.; Mathew, S.; Curchod, B. F. E. Dye-Sensitized Solar

Cells with 13% Efficiency Achieved through the Molecular Engineering of Porphyrin Sensitizers. *Nat. Chem.* **2014**, *6* (3), 242–247.

(4) Cao, Y.; Liu, Y.; Zakeeruddin, S. M.; Hagfeldt, A.; Gratzel, M. Direct Contact of Selective Charge Extraction Layers Enables High-Efficiency Molecular Photovoltaics Direct Contact of Selective Charge Extraction Layers Enables High-Efficiency Molecular Photovoltaics. *Joule* **2018**, No. 2, 1108–1117.

(5) Nazeeruddin, K. Efficient Panchromatic Sensitization of Nanocrystalline TiO2 Films by a Black Dye Based on a Trit.Pdf. *Chem. Commun.* **1997**, *1*, 1705–1706.

(6) Nazeeruddin, M. K.; Péchy, P.; Renouard, T.; Zakeeruddin, S. M.; Humphry-Baker, R.; Cointe, P.; Liska, P.; Cevey, L.; Costa, E.; Shklover, V.; et al. Engineering of Efficient Panchromatic Sensitizers for Nanocrystalline TiO2-Based Solar Cells. *J. Am. Chem. Soc.* **2001**, *123* (8), 1613–1624.

(7) Boschloo, G.; Hagfeldt, A.; Spectus, C. O. N. Characteristics of the Iodide / Triiodide Redox Mediator in Dye-Sensitized Solar Cells. *Acc. Chem. Res.* **2009**, *42* (11), 1819–1826.

(8) Hamann, T. W. The End of Iodide? Cobalt Complex Redox Shuttles in DSSCs. *Dalt. Trans.* **2012**, *41* (11), 3111–3115.

(9) Hao, Y.; Saygili, Y.; Cong, J.; Eriksson, A.; Yang, W.; Zhang, J.; Polanski, E.; Nonomura, K.; Zakeeruddin, S. M.; Grätzel, M.; et al. Novel Blue Organic Dye for Dye-Sensitized Solar Cells Achieving High Efficiency in Cobalt-Based Electrolytes and by Co-Sensitization. *ACS Appl. Mater. Interfaces* **2016**, *8* (48), 32797–32804.

(10) Vlachopoulos, N.; Pellet, N.; Cao, Y.; Zakeeruddin, S. M.; Giordano, F.; Söderberg, M.; Pavone, M.; Freitag, M.; Boschloo, G.; Kavan, L.; et al. Copper Bipyridyl Redox Mediators for Dye-Sensitized Solar Cells with High Photovoltage. *J. Am. Chem. Soc.* **2016**, *138* (45), 15087–15096.

(11) Wilkins, R. G. *Kinetics and Mechanism of Reactions of Transition Metal Complexes*; 2002; Vol. 5.

(12) Xie, Y.; Hamann, T. W. Fast Low-Spin Cobalt Complex Redox Shuttles for Dye-Sensitized Solar Cells. *J. Phys. Chem. Lett.* **2013**, *4* (2), 328–332.

(13) Xie, Y.; Baillargeon, J.; Hamann, T. W. Kinetics of Regeneration and Recombination Reactions in Dye-Sensitized Solar Cells Employing Cobalt Redox Shuttles. *J. Phys. Chem. C* **2015**, *119* (50), 28155–28166.

(14) Bechlars, B.; Alessandro, D. M. D.; Jenkins, D. M.; Iavarone, A. T.; Glover, S. D.; Kubiak, C. P.; Long, J. R. Divanadium Complexes. *Nat. Chem.* **2010**, *2* (5), 362–368.

(15) Kashif, M. K.; Axelson, J. C.; Duffy, N. W.; Forsyth, C. M.; Chang, C. J.; Long, J. R.; Spiccia, L.; Bach, U. A New Direction in Dye-Sensitized Solar Cells Redox Mediator Development: In Situ Fine-Tuning of the Cobalt(II)/(III) Redox Potential through Lewis Base Interactions. *J. Am. Chem. Soc.* **2012**, *134* (40), 16646–16653.

(16) Baillargeon, J.; Xie, Y.; Raithel, A. L.; Ghaffari, B.; Staples, R. J.; Hamann, T. W. Spin-Doctoring Cobalt Redox Shuttles for Dye-Sensitized Solar Cells. *Inorg. Chem.* **2018**, *57* (18), 11633–11645.

(17) Barham, J. P.; John, M. P.; Murphy, J. A. Contra-Thermodynamic Hydrogen Atom

Abstraction in the Selective C-H Functionalization of Trialkylamine N-CH3 Groups. *J. Am. Chem. Soc.* **2016**, *138* (47), 15482–15487.

(18) Hinz, A.; Schulz, A.; Villinger, A. Tunable Cyclopentane-1,3-Diyls Generated by Insertion of Isonitriles into Diphosphadiazanediyls. *J. Am. Chem. Soc.* **2015**, *137* (31), 9953–9962.

(19) Zadrozny, J. M.; Freedman, D. E.; Jenkins, D. M.; Harris, T. D.; Iavarone, A. T.; Mathonière, C.; Clérac, R.; Long, J. R. Slow Magnetic Relaxation and Charge-Transfer in Cyano-Bridged Coordination Clusters Incorporating [Re(CN)7]3-/4-. *Inorg. Chem.* **2010**, *49* (19), 8886–8896.

(20) Häggman, L.; Boschloo, G.; Ellis, H.; Vlachopoulos, N.; Perruchot, C.; Hagfeldt, A.; Jouini, M. PEDOT Counter Electrodes for Dye-Sensitized Solar Cells Prepared by Aqueous Micellar Electrodeposition. *Electrochim. Acta* **2013**, *107*, 45–51.

(21) Connelly, N. G.; Geiger, W. E. Chemical Redox Agents for Organometallic Chemistry. *Chem. Rev.* **1996**, *96*, 877–910.

(22) Setzer, W. N.; Ogle, C. A.; Wilson, G. S.; Glass, R. S. 1,4,7-Trithiacyclononane, a Novel Tridentate Thioether Ligand, and the Structures of Its Nickel(II), Cobalt(II), and Copper(II) Complexes. *Inorg. Chem.* **1983**, *22* (2), 266–271.

(23) Saito, Y.; Takemoto, J.; Hutchinson, B.; Nakamoto, K. Infrared Studies of Coordination Compounds Containing Low-Oxidation-State Metals. I. Tris(2,2′-Bipyridine) and Tris(l,10-Phenanthroline) Complexes. *Inorg. Chem.* **1972**, *11* (9), 2003–2011.

(24) Brunschwig, B. S.; Logan, J.; Newton, M. D.; Sutin, N. A Semiclassical Treatment of

Electron-Exchange Reactions. Application to the Hexaaquoiron(II)-Hexaaquoiron(III) System. *J. Am. Chem. Soc.* **1980**, *102* (18), 5798–5809.

(25) Sutin, N. *Theory of Electron Transfer Reactions: Insights and Hindsights*; 1983; Vol. 30.

(26) Jones, P. G. Crystal Structure Determination: A Critical View. 157–172.

(27) Lide, D. R.; Haynes, W. M. M.; Baysinger, G.; Berger, L. I.; Kehiaian, H. V; Roth, D. L.; Kuchitsu, K.; Zwillinger, D.; Frenkel, M.; Goldberg, R. N. CRC Handbook of Chemistry and Physics, 2009−2010, 90th Ed. *J. Am. Chem. Soc.* **2009**, *131* (35), 12862–12862.

(28) Marcus, R. A.; Sutin, N. Electron Transfers in Chemistry and Biology. *Biochim. Biophys. Acta* **1985**, *811*, 265–322.

(29) Tiwary, S. K.; Vasudevan, S. Spin Crossover in the Ship-in-a-Bottle Compound: Cobalt(II) Tris(Bipyridyl) Encapsulated in Zeolite-Y. *Chem. Phys. Lett.* **1997**, *277* (1–3), 84–88.

(30) Hamann, T. W.; Gstrein, F.; Brunschwig, B. S.; Lewis, N. S. Measurement of the Dependence of Interfacial Charge-Transfer Rate Constants on the Reorganization Energy of Redox Species at n-ZnO/H2O Interfaces. *J. Am. Chem. Soc.* **2005**, *127* (40), 13949–13954.

(31) Yao, J. C.; Ma, L. F.; Yao, F. J. Crystal Structure of Tris(2,2’ -Bipyridine)Cobalt(II) Diperchlorate,. *Z. Krist. NCS* **2005**, *220*, 483–484.

(32) Du, M.; Zhao, X. J.; Cai, H. Crystal Structure of Tris(2,2’-Bipyridine)Cobalt(in) Triperchlorate Dihydrate,. *Z. Krist. NCS* **2004**, *219*, 463–465.

(33) Katayama, Y.; Nakayama, S.; Tachikawa, N.; Yoshii, K. Electrochemical Behavior of

Tris(2,2′-Bipyridine)Cobalt Complex in Some Ionic Liquids . *J. Electrochem. Soc.* **2017**, *164* (8), H5286–H5291.

(34) Bella, F.; Galliano, S.; Gerbaldi, C.; Viscardi, G. Cobalt-Based Electrolytes for Dye-Sensitized Solar Cells: Recent Advances towards Stable Devices. *Energies* **2016**, *9* (5), 1–22.

(35) Ellis, H.; Eriksson, S. K.; Feldt, S. M.; Gabrielsson, E.; Lohse, P. W.; Lindblad, R.; Sun, L. Linker Unit Modification of Triphenylamine-Based Organic Dyes For. *J. Phys. Chem. C* **2013**, *117*, 21029–21036.

(36) Cong, J.; Hao, Y.; Boschloo, G.; Kloo, L. Electrolytes Based on TEMPO – Co Tandem Redox Systems Outperform Single Redox Systems in Dye-Sensitized Solar. *ChemSusChem* **2015**, *8*, 264–268.

(37) Robson, K. C. D.; Hu, K.; Meyer, G. J.; Berlinguette, C. P. Atomic Level Resolution of Dye Regeneration in the Dye-Sensitized Solar Cell. *J. Am. Chem. Soc.* **2013**, *135*, 1961–1971.

(38) Cong, J.; Hao, Y.; Sun, L.; Kloo, L. Two Redox Couples Are Better Than One : Improved Current and Fill Factor from Cobalt-Based Electrolytes in Dye-Sensitized Solar Cells. *Adv. Energy Mater.* **2014**, *4*, 1–6.

(39) Yang, W.; Vlachopoulos, N.; Boschloo, G. Impact of Local Electric Fields on Charge-Transfer Processes at the TiO2 /Dye/Electrolyte Interface. *ACS. Energy Lett.* **2017**, *2*, 161–167.

(40) Feldt, S. M.; Wang, G.; Boschloo, G.; Hagfeldt, A. Effects of Driving Forces for

Recombination and Regeneration on the Photovoltaic Performance of Dye-Sensitized Solar Cells Using Cobalt Polypyridine Redox Couples. *J. Phys. Chem. C* **2011**, *115*, 21500–21507.

(41) Tachibana, Y.; Koumura, N.; Bach, U.; Spiccia, L. Dye Regeneration Kinetics in Dye-Sensitized Solar Cells. *J. Am. Chem. Soc.* **2012**, *134*, 16925–16928.

(42) Ellis, H.; Schmidt, I.; Hagfeldt, A.; Wittstock, G.; Boschloo, G. Influence of Dye Architecture of Triphenylamine Based Organic Dyes on the Kinetics in Dye-Sensitized Solar Cells. *J. Phys. Chem. C* **2015**, *119*, 21775–21783.

(43) Marinado, T.; Hagberg, D. P.; Hedlund, M.; Edvinsson, T.; Brinck, T.; Johansson, E. M. J.; Boschloo, G. Rhodanine Dyes for Dye-Sensitized Solar Cells : Spectroscopy , Energy Levels and Photovoltaic Performance. *Phys. Chem. Chem. Phys.* **2009**, *11*, 133–141.

(44) Fabregat-Santiago, F.; Garcia-Belmonte, G.; Mora-Seró, I.; Bisquert, J. Characterization of Nanostructured Hybrid and Organic Solar Cells by Impedance Spectroscopy. *Phys. Chem. Chem. Phys.* **2011**, *13* (20), 9083–9118.

(45) Hao, Y.; Yang, W.; Zhang, L.; Jiang, R.; Mijangos, E.; Saygili, Y.; Hammarström, L.; Hagfeldt, A.; Boschloo, G.; O'Regan, B.; et al. A Small Electron Donor in Cobalt Complex Electrolyte Significantly Improves Efficiency in Dye-Sensitized Solar Cells. *Nat. Commun.* **2016**, *7*, 13934.

(46) Raga, S. R.; Barea, E. M.; Fabregat-Santiago, F. Analysis of the Origin of Open Circuit Voltage in Dye Solar Cells. *J. Phys. Chem. Lett.* **2012**, *3* (12), 1629–1634.

(47) Ondersma, J. W.; Hamann, T. W. Measurements and Modeling of Recombination from

Nanoparticle TiO2 Electrodes. *J. Am. Chem. Soc.* **2011**, *133* (21), 8264–8271.

(48) Balraju, P.; Suresh, P.; Kumar, M.; Roy, M. S.; Sharma, G. D. Effect of Counter Electrode , Thickness and Sintering Temperature of TiO2 Electrode and TBP Addition in Electrolyte on Photovoltaic Performance of Dye Sensitized Solar Cell Using Pyronine G (PYR) Dye. *J. Photochem. Photobiol.* **2009**, *206*, 53–63.

(49) Katz, M. J.; Vermeer, M. J. D.; Farha, O. K.; Pellin, M. J.; Hupp, J. T. Effects of Adsorbed Pyridine Derivatives and Ultrathin Atomic-Layer- Deposited Alumina Coatings on the Conduction Band-Edge Energy of TiO2 and on Redox-Shuttle-Derived Dark Currents. *Langmuir* **2013**, *29*, 806–814.

(50) Hamann, T. W.; Jensen, R. A.; Martinson, A. B. F.; Ryswyk, V.; Hupp, J. T.; Hamann, T. Advancing beyond Current Generation Dye-Sensitized Solar Cells. *Energy Environ. Sci.* **2008**, *1*, 66–78.

Table of Contents Graphic: The electron transfer kinetics in the DSSCs were tuned dramatically by coordination of the strong-field ligand 2,6-dimethyl isocyanide to induce a low-spin Co(II) redox shuttle.